CHEMISTRY
A EUROPEAN JOURNAL

ChemPubSoc
Europe

DOI: 10.1002/chem.201102828

What Controls the Magnetic Interaction in bis-μ-Alkoxo Mn^{III} Dimers? A Combined Experimental and Theoretical Exploration

Nelly Berg,[a] Thayalan Rajeshkumar,[b] Stephanie M. Taylor,[c] Euan K. Brechin,[c] Gopalan Rajaraman,*[b] and Leigh F. Jones*[a]

In memory of Janis Purves Jones

Abstract: The synthesis and magnetic characterisation of a series of bis-μ-alkoxide bridged Mn^{III} dinuclear complexes of general formula $[Mn^{III}_2(\mu\text{-}OR)_2(biphen)_2(ROH)_x(L)_y]$ (where R = Me, Et; H_2biphen = 2,2′-biphenol and L = terminally bonded N-donor ligand) is described, doubling the literature basis set for this type of complex. Building on these findings we have categorised all known μ-OR bridged Mn^{III} dinuclear complexes into one of three classifications with respect to their molecular structures. We have then employed DFT and MO calculations to assess all potential magneto-structural correlations for this class of compound in order to identify the structural requirements for constructing ferromagnetic family members. Our analysis indicates that the most influential parameter which governs the exchange interaction in this class of compounds is the relative orientation of the JT axes of the Mn^{III} atoms. A perpendicular orientation of the JT axes leads to a large ferromagnetic contribution to the exchange. These results also suggest that a large ferromagnetic interaction and a large anisotropy are unlikely to coexist in such structural types.

Keywords: coordination complexes · density functional calculations · magneto-structural correlations · manganese · molecular magnetism

Introduction

The construction of families of polynuclear cluster compounds containing multiple paramagnetic metal centres and the understanding and development of the relationship between structure and magnetism (magneto-structural correlations) is an area of widespread interest.[1] In practice of course this is not a trivial task, even assuming that a large number of structurally-related compounds can be synthesised, crystallised and characterised, because the super-exchange mechanisms involved are influenced by many structural factors including, for example, the type of metal ion(s) (M) and bridging ligand(s) (L) employed, and the specific M−M and M−L distances and the M-L-M and M-L-L-M angles in the molecule.[1] Despite these obstacles such studies are extremely important because the ability to control and modulate the type and magnitude of magnetic exchange within a complex has enormous ramifications for materials science and nanotechnology.[2] Seminal work in this field emerged shortly after the discovery of the apparent anomalous paramagnetism of "monomeric" copper acetate.[3] The molecular structure was proposed to be dimeric by Bleaney and Bowers in 1952 using EPR spectroscopy[4] and was later validated via single crystal X-ray diffraction.[5] These findings coincided with the rapid development of structure determination and soon led to the evolution of magneto-structural correlation studies within other dinuclear Cu^{II} species. The first example of a quantitative relationship was developed by Hatfield and Hodgson in a large family of di-μ-OH^- bridged $[Cu^{II}_2]$ complexes, in which the magnetic exchange (J) was found to be governed by the magnitude of the Cu-OH-Cu angle.[6] These observations were then followed by other studies on dimeric cupric complexes containing, for example, symmetric halide bridging ligands,[7] asymmetric mixed ligand combinations,[8] and a family of end-on azide-bridged complexes containing both ferro- and antiferromagnetically coupled siblings in which the magnetic exchange was very elegantly shown to depend on the Cu-N-Cu angle.[9] Thereafter, magneto-structural correlations were also attempted and established for (dimeric) complexes containing other first row transition metal ions such as Fe^{III},[10] Cr^{III},[11] Mn^{II}[12] and Mn^{III}.[13]

[a] N. Berg, Dr. L. F. Jones
School of Chemistry
NUI Galway
University Road, Galway (Ireland)
E-mail: leigh.jones@nuigalway.ie

[b] T. Rajeshkumar, Dr. G. Rajaraman
Department of Chemistry
Indian Institute of Technology
Powai, Mumbai, 400 076 (India)
E-mail: rajaraman@chem.iitb.ac.in

[c] S. M. Taylor, Prof. E. K. Brechin
EaStCHEM School of Chemistry
University of Edinburgh
West Mains Rd, Edinburgh, EH9 3JJ (UK)

Supporting information for this article is available on the WWW under http://dx.doi.org/10.1002/chem.201102828.

Understanding the magneto-structural relationship in small compounds, such as dimers and trimers, is also an important step towards understanding the magnetic behaviour of large or very large polymetallic complexes, since the magnetic skeletons of the latter are often made up of the same basic building blocks. Recent trends in molecular magnetism have seen enormous growth in the synthesis of molecules containing tens, if not hundreds, of metal ions because of their potential application in, for example, information storage, magnetic refrigeration, quantum information processing and molecular spintronics.[14] Such compounds often possess very elaborate topologies comprising multiple M-L-M and/or M-L-L-M exchange pathways that may not be accurately deciphered due to over parameterisation and/or computational limitations.[15] However, if the magnetic behaviour of the small building blocks that self-assemble to form the larger architecture are known and understood, the magnetic behaviour of the larger molecule can be more easily rationalised. Indeed the last few years have seen both qualitative and quantitative magneto-structural trends established for tri-,[16] tetra-,[15a,17] hexa-,[18] and octanuclear[19] complexes of first row transition metals, as well as with mixed metal 3d–4f species.[20]

In addition to experimental observations, theoretical methods based on density functional theory have become increasingly popular tools with which to compute magnetic exchange interactions and develop magneto-structural correlations.[21] Established theoretical protocols have provided excellent numerical estimates of J values and of the underlying electronic structure. One major advantage of the theoretical approach is that magneto-structural correlations for a particular structure type can be developed on simplified model complexes in which structural parameters can be modified in a methodical manner, offering insights into the effect of one particular structural change at a time on the sign and magnitude of J.

Due to its large single ion anisotropy the Jahn–Teller distorted Mn^{III} ion is often the metal of choice for the synthesis of Single-Molecule Magnets (SMMs), an important class of compounds with potential application in information storage.[14,22] To build such molecules it is preferable to have strong ferromagnetic exchange between neighbouring Mn centres and as such knowledge of what controls the pairwise magnetic exchange is vital. A literature search reveals however that the majority of di- and polynuclear Mn^{III} complexes exhibit, with few exceptions,[46,47] very weak ferro- or antiferromagnetic exchange interactions and that the parameters that control the magnitude and sign of J have not been clearly established - even for simple Mn^{III} dimers. The bis-alkoxo bridged dinuclear Mn^{III} compounds reported in the literature to date are collected in Table 2, Table 3 and Table 4, and have J values (based on the $-2JS_i \cdot S_j$ formalism) ranging from $-15.5\ cm^{-1}$ to $+19.7\ cm^{-1}$. Herein, we describe the synthesis and magnetic characterisation of a new family of bis-μ-alkoxide bridged Mn^{III} dinuclear complexes of general formula $[Mn^{III}_2(\mu\text{-}OR)_2(biphen)_2(ROH)_x(L)_y]$ (where R = Me, Et; H_2biphen = 2,2′-biphenol and L = terminally bonded N-donor ligand) and establish a magneto-structural correlation for all known bis-alkoxo bridged dinuclear Mn^{III} compounds using a combined experimental and theoretical study.

Results and Discussion

All significant bond distances and angles along with single crystal X-ray diffraction data for complexes **1**–**5** are given in Table 1 and S1 in the Supporting Information, respectively. Structural parameters pertinent to our correlation studies are given in Table 2, Table 3 and Table 4. The first member of this family is $[Mn^{III}_2(\mu\text{-}OMe)_2(biphen)_2(MeOH)_4]$ (**1**), formed via the reaction of $Mn(NO_3)_2{\cdot}6H_2O$, 2,2′-biphenol[23] and NaOH in alcohol. Complex **1** (Figure 1) crystallises in the triclinic $P\bar{1}$ space group with an asymmetric unit composed of one dinuclear molecule. The two six-coordinate Mn^{III} ions, which lie about an inversion centre (Mn1 and symmetry equivalent (s.e.)), are bridged via two μ-OMe anions with a Mn1-O1-Mn1′ angle of 103.66° and Mn1···Mn1′ distance of 3.071 Å. Each Mn^{III} cation is ligated by two oxygen atoms from a chelating, doubly deprotonated 2,2′-biphenolate ligand. The six coordinate distorted octahedral geometries of each metal ion are completed by two terminal methanol molecules which bond on the Jahn–Teller axes at distances of 2.37 Å (Mn1−O4) and 2.27 Å (Mn1−O5). The oxidation state of the Mn^{III} was confirmed through bond length and charge balance considerations and BVS calculations (as were all others described in this work).

The introduction of N-donor (pyridine type) ligands into the synthetic procedure used for the formation of **1** gives rise to the remaining members of this family. For instance,

Table 1. Selected bond lengths (Å) and angles (°) for complexes **1**–**5**.

	1		**2**		**3**		**4**		**5**
Mn1−O1	1.956(19)	Mn1−O1	1.972(6)	Mn1−O1	1.938(2)	Mn1−O1	1.9388(14)	Mn1−O1	1.9372(15)
Mn1−O1#	1.950(2)	Mn1−O2	1.936(2)	Mn1−O1#	1.935(2)	Mn1−O1#	1.9475(14)	Mn1−O1#	1.9496(15)
Mn1−O2	1.896(2)	Mn1−O3	1.841(6)	Mn1−O2	1.853(2)	Mn1−O2	1.8363(15)	Mn1−O2	1.8563(14)
Mn1−O3	1.852(2)	Mn1−O4	1.879(6)	Mn1−O3	1.842(2)	Mn1−O3	1.8645(15)	Mn1−O3	1.8839(15)
Mn1−O4	2.366(3)	Mn1−N1	2.321(7)	Mn1−N1	2.196(2)	Mn1−N1	2.1847(19)	Mn1−O4	2.3056(16)
Mn1−O5	2.270(2)	Mn1−N2	2.420(8)					Mn1−O5	2.2839(16)
Mn1-O1-Mn1#	103.65(10)	Mn1-O1-Mn1#	101.1(2)	Mn1-O1-Mn1#	104.11(9)	Mn1-O1-Mn1#	103.03(6)	Mn1-O1-Mn1#	102.85(6)
Mn1···Mn1#	3.071	Mn1···Mn1#	3.007(2)	Mn1···Mn1#	3.0537(9)	Mn1···Mn1#	3.0422(8)	Mn1···Mn1#	3.039

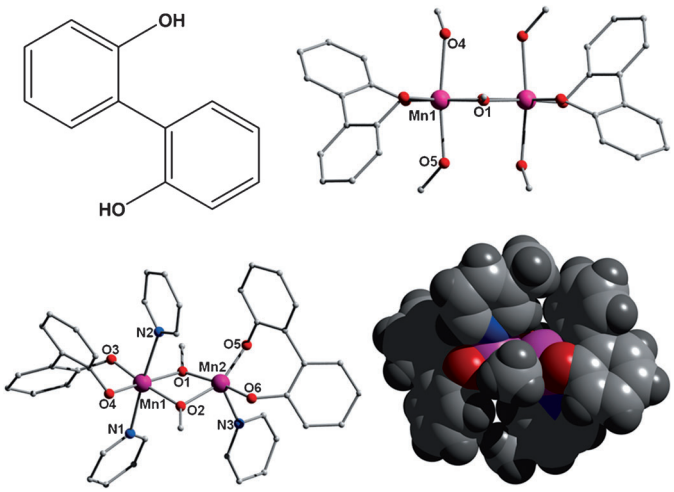

Figure 1. Schematic of 2,2′-biphenol (top left), crystal structure of **1** (top right), crystal structure of **2** viewed as ball-and stick (bottom left) and space-fill (bottom right). Pink = Mn, red = O, blue = N, light grey = C, dark grey = H.

the addition of pyridine (py) and 3-picoline (3-pic) affords $[Mn^{III}_2(\mu\text{-}OMe)_2(biphen)_2(py)_3]$ (**2**) and $[Mn^{III}_2(\mu\text{-}OMe)_2(biphen)_2(3\text{-}pic)_2]\cdot 2H_2O$ (**3**), respectively. Complexes **2** and **3** (Figure 1 and Figure 2) crystallise in the monoclinic space groups $P2_1/c$ and C_2/c respectively and share many structural similarities with complex **1**. Both contain central μ-OMe^- ligands, this time producing Mn^{III}-O-Mn^{III} angles of 101.14° (Mn1-O1-Mn2) and 100.70° (Mn1-O2-Mn2) in **2** and 104.04° (Mn1-O1-Mn1′) in **3**. Indeed **2** and **3** differ to complex **1** only in the presence of terminally bonded N-donor ligands rather than terminally bonded alcohol. More specifically, complex **2** contains two pyridine ligands axially coordinated to the Jahn–Teller axis of [distorted octahedral] Mn1 (via N1 and N2), and one pyridine molecule attached (N3) to Mn2. The latter is in a distorted square based pyramidal geometry ($\tau = 0.28$),[24] presumably due to the steric effects of the rather twisted biphenoxide ligands (Figure 1). The Mn1–N1 and Mn1–N2 bond lengths in **2** are 2.322 Å and 2.420 Å respectively, while the Mn–N3 distance is slightly shorter, at a value of 2.207 Å. The steric constraints present in **2** give rise to a puckering of the $\{Mn^{III}_2(\mu\text{-}OMe)_2\}$ plane. This core distortion can be quantified via the Mn1-O1-Mn2-O2 torsion angle of 15.08° which can be directly compared to the completely flat $\{Mn^{III}_2(\mu\text{-}OMe)_2\}$ plane in complex **1** (Mn1-O1-Mn1′-O′ = 0.0°). The individual $\{Mn_2\}$ units in **1** stack in superimposable rows along the *a* axis of the unit cell (Figure S1 in the Supporting Information). These 1-D rows are stabilised by two symmetry related H-bonding interactions between an O atom of a $biphen^{2-}$ ligand (O2) and a nearby alcoholic proton (H4A-O4) belonging to a terminal EtOH ligand of a juxtaposed {Mn2} unit (O2···H4A(O4) = 1.909 Å). These hydrogen bonded chains arrange in the common brickwork pattern in the remaining two directions. No significant intermolecular interactions are observed between the chains in **1**. The packing arrangement in **2** also comprises superimposable 1-D rows propagating along the *c* axis of the unit cell. These chains are held in position by only weak interactions; however these rows are connected in 3-dimensions via strong C–H···π dipolar interactions at a distance of 2.496 Å ([C24–C29]···H4(C4)) emanating from biphenolate and pyridyl aromatic rings on neighbouring dimeric units.

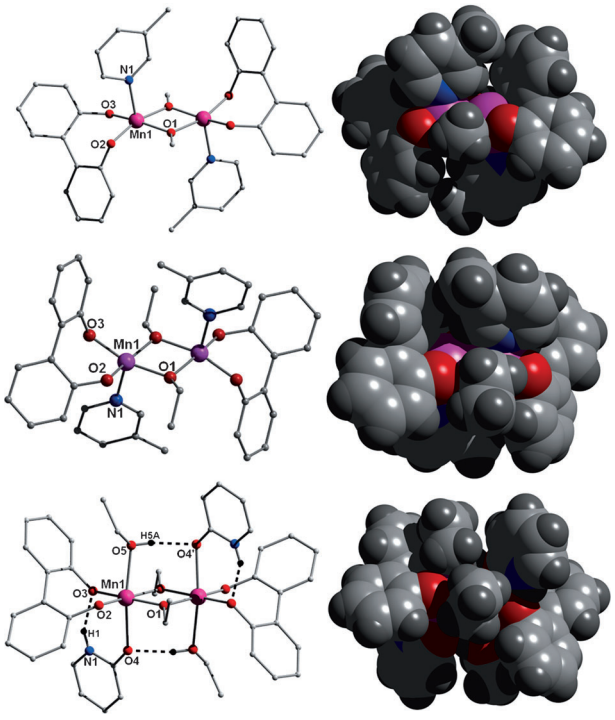

Figure 2. Crystal structures and equivalent space-fill representations of complexes **3**–**5** (top→bottom). Colour code as in Figure 1. H atoms have been omitted for clarity. Dashed lines represent intramolecular H-bonding interactions (N1(H1)···O3 = 1.913 Å).

In complex **3** (Figure 2) both Mn^{III} ions are five coordinate and adopt square-based pyramidal geometry ($\tau = 0.02$), with one 3-picoline ligand coordinated to each metal centre at a distance of 2.198 Å (Mn1–N1). This change in metal coordination number is presumably due to the presence of the bulkier 3-picoline ligand (Figure 2). This is also true for $[Mn^{III}_2(\mu\text{-}OEt)_2(biphen)_2(3\text{-}pic)_2]$ (**4**) (Figure 2), whose structure is essentially analogous to complex **3** but in which the bridging methoxide ions are replaced with bridging ethoxide ligands, as a result of the change of solvent from MeOH to EtOH. **4** crystallises in monoclinic space group $P2_1/n$. The Mn-O-Mn angles in **3** and **4** are given as 104.11 and 103.03° resulting in Mn···Mn distances of 3.054 and 3.402 Å, respectively. Moreover the Mn-O-Mn-O torsion angles produced in **3** and **4** are both 0°. The crystal packing in the unit cells of **3** and **4** bear striking similarities. Both comprise 1-D superimposable chains running across (dissecting) the *ab* plane in **3** and along the *b* axis in **4**. The individual $\{Mn_2\}$ units in these siblings are connected through intrachain H-bonding interactions via O atoms and methyl protons belonging to biphenolate and 3-picoline ligands, respectively, of nearest neighbour $[Mn_2]$ units (O3···H18A(C18) = 2.715 Å in **3**;

O2···H19(C19) = 2.420 Å in **4**). In terms of 3-D connectivity the 1-D rows in **3** and **4** each alternate in direction along the *c* axis of their unit cells. Inter-chain close contacts were observed in both structures via interactions between O and H atoms of neighbouring biphen^{2-} bridging ligands (O2···H9(C9) = 2.550 Å in **3**; O2···H19(C19) = 2.420 Å in **4**) (Figure S3 in the Supporting Information). The final member of the family, $[Mn^{III}_2(\mu\text{-OEt})_2(biphen)_2(2\text{-O-pyH})_2]$ (**5**; Figure 3), is made from the reaction of $Mn(ClO_4)_2{\cdot}6H_2O$,

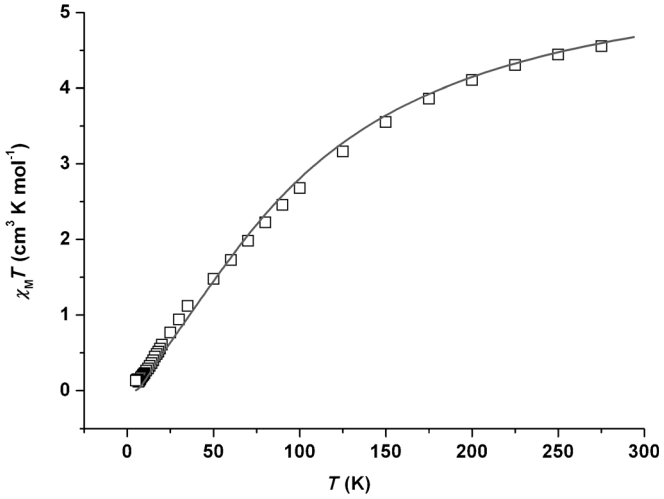

Figure 3. Plot of magnetic susceptibility ($\chi_m T$) vs. T for complex **4**. The solid line represents the best-fit using the parameters provided in Table 2. See the Supporting Information for the magnetic susceptibility plots of complexes **1**–**3** and **5**.

2,2′-biphenol, 2-hydroxypyridine (2-OH-py) and NMe_4OH in EtOH. The common central {Mn-(μ-OEt)$_2$-Mn} core is retained, with a Mn1-O1-Mn1′ angle of 102.85° and a Mn···Mn distance of 3.039 Å (Mn-O-Mn-O torsion angle = 0°). Indeed the only major structural difference between **5** and its siblings lies in the nature of the bonding of the 2-hydroxypyridine ligands; the ligand bonds to the metal centre via the deprotonated phenolic O-atom (Mn1−O4, 2.306 Å), with the pyridyl N atom now protonated and H-bonding to an O-atom of the chelating biphenoxide (N1(H1)···O3 = 1.913 Å). A second intramolecular H-bond is observed between the terminal EtOH ligands, that complete the octahedral coordination spheres at each Mn^{III} centre, and O4 (O5(H5)···O4′, 1.907 Å). Akin to the other family members, the {Mn_2} units in **5** connect into chains (dissecting the *ab* plane of the cell) via two symmetry equivalent C−H···π close contacts ((C17−C21)···H16(C16) = 3.293 Å), derived from interactions between aromatic pyridyl ring and ethyl protons of a close by terminal EtOH molecule (Figure S3 in the Supporting Information). Furthermore, these 1-D rows further connect in the remaining directions via further C−H···π interactions comprising aromatic rings and aromatic protons of juxtaposed biphenolate ligands of neighbouring [Mn_2] complexes ([C9−C14]···H7(C7) = 2.583 Å).

Magnetic susceptibility measurements: Magnetic susceptibility measurements on complexes **1**–**5** were carried out in the 300–5 K temperature range in an applied field of 0.1 T (Figure 3). The room temperature $\chi_M T$ products for **1**–**5** lie in the 4.03–4.55 cm^3 mol^{-1} K range and are significantly lower than the expected value for two non-interacting Mn^{III} ions of 6.00 cm^3 mol^{-1} K, assuming $g = 2.00$. This is an indication of antiferromagnetic exchange between the metal centres, as supported by the uniform drop in $\chi_M T$ on decreasing temperature. In each case, the $T = 5$ K value is close to zero. Fitting of these data with a simple 1 *J* isotropic Hamiltonian ($\hat{H} = -2J\hat{S}_1{\cdot}\hat{S}_{1'}$) affords the best fit parameters documented in Table 2 and represented by the solid lines in Figure 3 and S4 in the Supporting Information. The *J* values span the small range of −10.5 cm^{-1} (in **4**) to −14.3 cm^{-1} (in **3**).

To put these results into context we have compared the structural and magnetic properties of **1**–**5** to those of all

Table 2. Selected magneto-structural parameters for type I Mn^{III} dinuclear complexes discussed in this work and elsewhere. Magnetic data is reported in the $\hat{H} = -2J\hat{S}_1{\cdot}\hat{S}_{1'}$ formalism.

Formula	*g*	*J* value (exptl) [cm^{-1}]	*J* value (calcd) [cm^{-1}]	Mn···Mn [Å]	Mn-O-Mn angle [Å][a]	Mn-O-Mn-O torsion	JT dihedral [Å]	Mn−O [Å][a]	Ref.
$[Mn_2(OMe)_2(L)_2(MeOH)_4]$ (**1**)	1.98	−12.2	−10.5	3.071	103.66	0	5.4	1.953	t. w.
$[Mn2(OMe)_2(L)_2(py)_3]$ (**2**)	1.98	−12.5	–	3.007	100.93	15.37	–	1.950	t. w.
$[Mn_2(OMe)_2(L)_2(3\text{-pic})_2]$ (**3**)	1.98	−14.3	–	3.054	104.04	0	–	1.936	t. w.
$[Mn_2(OEt)_2(L)_2(3\text{-pic})_2]$ (**4**)	1.98	−10.5	−12.4	3.042	103.03	0	0	1.944	t. w.
$[Mn_2(OEt)_2(L)_2(hpy)_2(EtOH)_2]$ (**5**)	1.98	−13.5	−11.6	3.039	102.85	0	0	1.944	t. w.
$[Mn_2(L)(OMe)(OAc)(MeOH)_2]Br$	1.90	−13.1	–	2.942	97.86	14.85	0.6	1.952	[25]
$[Mn_2(3\text{-OMe-salpentO})(OMe)(OAc)(MeOH)_2]Br$	1.98	−13.7	–	2.928	98.11	15.10	3.3	1.938	[26]
$[Mn_2(5\text{-}NO_2\text{-salpentO})(OMe)(OAc)(MeOH)_2]I_3$	1.98	−12.4	–	2.911	97.95	15.75	4.5	1.930	[27]
$[Mn_2(L^{Se})_2(OMe)_2(MeOH)_2]$	2.00	−11.8	–	3.038	102.57	7.06	6.5	1.947	[28]
$[Mn_2(L^{S})_2(OMe)_2(MeOH)_2]$	2.00	−8.2	–	n.c.a.	n.c.a.	n.c.a.	–	n.c.a.	[28]
$[Mn_2(3\text{-Me-salpentO})(OMe)(OAc)(MeOH)_2]Br$	2.02	−15.1	–	2.929	98.22	16	0	1.937	[29]
$[Mn_2(L)(OMe)Cl_2(MeOH)_2]$	2.00	−15.5	–	3.006	101.50	n.c.a	–	1.941	[30]
$[Mn_2(OMe)_2(sal)_2(MeOH)_4]$	2.00	−10.33	–	3.025	102.97	0	5.2	1.934	[31]

[a] average values. t.w = this work; n.c.a = no coordinates available.

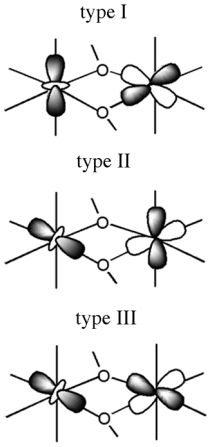

Figure 4. Schematic illustrating the three types of magnetic orbital spatial orientations observed within recognised μ-OR bridged $[Mn^{III}_2]$ complexes. Complexes **1**–**5** are classified as type I as described in this work.

known μ-OR bridged $[Mn^{III}_2]$ clusters reported in the literature. Each compound may be grouped into one of three distinct categories (see type I–III in Figure 4) based on the orientation of the Jahn–Teller axes,[25–50] using an approach proposed by Tuchagues and coworkers in 1995.[43] Each of these three families can be categorised by noting the relative orientation of their associated Jahn–Teller axes with respect to one another as well as their orientation with respect to the μ-OR bridging plane (Figure 4). These classifications are reported in Table 2, Table 3 and Table 4 along with their associated magnetic spin Hamiltonian parameters (*J*- and *g*-values; ground spin state *S*), and all structural parameters which may have a significant bearing on their resultant magnetic properties. These parameters were then utilised in our subsequent magneto-structural correlation studies (see above).

Type I: Complexes belonging to the first category exhibit a co-linear orientation of their Jahn–Teller axes, each of which are perpendicular to the bridging plane of the dimer as observed here and elsewhere in the literature (Figure 4). Indeed the introduction of complexes **1**–**5** almost doubles the literature basis set for this type of dinuclear species. Magnetic exchange parameters (*J*) for these compounds are all weakly antiferromagnetic with values ranging from $-8.2\ cm^{-1}$ to $-15.5\ cm^{-1}$.[28,30] Interestingly, a group of O^{2-} bridged $[Mn^{III}_2O_2]$ complexes exhibiting type I conformations are known. As these compounds possess μ-O^{2-} bridging anions rather than μ-OR^{-} species they are exempt from our comparative study. The μ-O^{2-} bridging angles of these dimers are significantly more acute than the μ-OR analogues (ca. 93–95°), leading to much shorter Mn···Mn distances (ca. 2.65-2.7 Å) and as a result these compounds exhibit strong antiferromagnetic interactions with *J* values of about $100\ cm^{-1}$.[51]

Type II: This is the most common conformation exhibited by alkoxide bridged dinuclear Mn^{III} complexes. Here, the Jahn–Teller axes of the Mn^{III} ions are parallel to one another as well as being parallel to the bridging μ-OR plane (Figure 4). The Mn−OR bonds in these types of complexes are thus elongated and as a result the extent of orbital overlaps amongst d-based orbitals appears to be altered. Indeed this may explain the magnetic coupling observed within these species as they exhibit magnetic exchange parameters which lie on the ferro↔antiferromagnetic interface. For instance, *J* values ranging from the weakly antiferromagnetic ($-1.68\ cm^{-1}$) in $[Mn_2(L)_2(H_2O)_2](ClO_4)_2$; where L = N-(acetylacetonylidene)-*N*′-α-methylsalicylidene,[43] to weakly ferromagnetic ($J = +6.3\ cm^{-1}$) in the complex $[Mn_2(salen)_2(H_2O)_2](ClO_4)_2$ where H_2salen = *N*,*N*′-bis(salicylideneaminoato)ethylene,[34] have been reported (Table 3).

Type III: Here the Jahn–Teller axes of the metal ions are perpendicular to one another: one lying parallel to the bridging plane, the other perpendicular to it (Figure 4). Just two alkoxide bridged $[Mn^{III}_2]$ complexes exhibiting this conformation have been reported to date. Furthermore both complexes exhibit relatively strong ferromagnetic coupling, proposed due to the non-colinearity of their respective elongated axes.[49,50] The rarity of these compounds is perhaps due to the low level of symmetry this conformation requires, with the complexes possessing different ligands at each of their two Mn^{III} centres (Table 4).

Since only the orientation between the two planes differs in the three types, we have defined a dihedral plane between the two Jahn–Teller axes which emerges as the key structural factor governing the differences in magnetic behaviour between types I–III and this parameter clearly defines the three categories of structures noted above. The collected experimental structures are plotted in Figure 5 as *J* versus dihedral plane. The way the dihedral angle has been measured within the dihedral plane is shown in Figure 5 (solid blue lines). As per our classification, all three types can be clearly distinguished. This is not true for any other structural parameters such as short/long Mn−O distances (where a scattered picture emerges). Accordingly, type I structures have dihedral planes $<10°$, type II structures fall into the 152–180° range and type III structures (where a strong ferromagnetic exchange has been observed) fall in the middle ground with dihedral angles of 81.9 and 117.1° for the two structures reported (Figure 5).

As is apparent from Table 2, Table 3, Table 4 and Figure 5 the magnitude of the exchange interaction *J* varies across the three types I–III. To understand in detail the difference in sign and magnitude of *J* observed among these structures and also to develop magneto-structural correlations based on other structural parameters, an extensive theoretical study based on density functional methods has been undertaken.

Theoretical studies: To explain the variation in magnetic behaviour between the three types of complexes presented here, we have carried out DFT calculations on selected structures from type I (**1**, **4** and **5**) type II (II-**1**, II-**2**) and type III (III-**1**, III-**2**). The computed *J* values are given in Table 2, Table 3 and Table 4. As is evident from the presented data the *J* values calculated are in good agreement with the experimentally reported values for these complexes. In fact, apart from complex III-**2**, excellent agreement in terms of the sign and magnitude of *J* has been observed in all the computed cases. The chosen method and the theoretical level are also able to effectively reproduce the magnitude

Table 3. Selected magneto-structural parameters for type II Mn^{III} dinuclear complexes discussed in this work and elsewhere. Magnetic data is reported in the $\hat{H} = -2J\hat{S}_1 \cdot \hat{S}_{1'}$ formalism.

Formula	*g*	*J* value (exptl) [cm^{-1}]	*J* value (calcd) [cm^{-1}]	Mn···Mn [Å]	Mn-O-Mn angle [Å][a]	Mn-O-Mn-O torsion	JT dihedral [Å]	Mn−O [Å][a]	Ref.
$[Mn_2(bbml)_2(acac)_2](BF_4)_2$	1.97	−0.18	–	3.178	105.27	n.c.a	–	1.99	[32]
$[Mn_2(saltmen)_2(ReO_4)_2]$	2.00	+1.84	–	3.330	98.00	0	–	2.193	[33]
$[Mn_2(salen)_2(H_2O)_2](ClO_4)_2$	2.00	+6.30	–	3.334	100.59	0	180	2.156	[34]
$[Mn_2(saltmen)_2(O_2CMe)_2]$	1.98	+1.35	0.73	3.641	99.57	0	152.5	2.352	[35a]
$[Mn_2(saltmen)_2(N_3)_2]$	1.98	+0.60	–	3.922	98.39	0	180	2.527	[35b]
$[Mn_2(salen)_2(NCO)_2]$	2.03	+0.73	–	3.584	97.82	0	180	2.346	[35c]
$[Mn(3,5\text{-Br-salen})(3,5\text{-Br-salicylal})]_2$	2.00	+0.55	–	3.597	100.00	0	180	2.323	[35d]
$[Mn_2(5\text{-Br-salen})_2(MeOH)_2](ClO_4)_2$	1.96	−0.45	−0.62	3.307	99.85	0	180	2.152	[35e]
$[Mn_2(L)_2(H_2O)_2](ClO_4)_2$	2.01	−1.68	–	3.318	103.38	0	180	2.109	[36]
$[Mn_2(Hthme)_2(bpy)_2](ClO_4)_2$	1.71	+2.13	–	3.096	101.56	0	180	1.996	[37]
$[Mn_2(L_1)_2(N_3)_2]$	2.04	−0.55	–	3.341	101.84	0	180	2.144	[38a]
$[Mn_2(L_2)_2(N_3)_2]$	1.99	+1.32	–	3.361	96.76	0	180	2.375	[38b]
$[Mn_2(OMe)_2(dbm)_4]$	1.98	+0.28	–	3.104	101.21	0	180	2.005	[39]
$[Mn_2(2\text{-OH}(5\text{-}NO_2\text{-sal})pn)_2]$	1.95	−5.0	–	3.247	99.07	0	180	2.127	[40]
$[Mn_2(bbml)_2(tol)_2](ClO_4)_2$	1.97	−1.19	–	3.209	106.29	0	177.9	2.004	[41]
$[Mn_2(saltmen)_2(H_2O)_2](ClO_4)_2$	1.93	+1.79	–	3.381	101.58	0	180	2.172	[42a]
$[Mn_2(naphtmen)_2(H_2O)_2](ClO_4)_2$	1.96	+1.20	–	3.541	100.59	0	180	2.279	[42b]
$[Mn_2(saltmen)_2(NCS)_2](ClO_4)_2$	1.99	+0.55	–	4.092	96.24	0	180	2.657	[42c]
$[Mn_2(napthmen)_2(NCS)_2](ClO_4)_2$	2.03	+0.12	–	4.388	96.57	0	180	2.818	[42d]
$[Mn_2(napthmen)_2(Cl)_2](ClO_4)_2$	2.04	+0.38	–	4.102	94.20	0	180	2.699	[42e]
$[Mn_2(3\text{-}NO_2\text{-salpro})_2(H_2O)].H_2O$	2.04	−1.62	–	3.223	100.52	0	180	2.095	[43]
$[Mn_2(salpn)_2(NCO)_2]$	2.02	0.42	–	3.429	100.58	0	180	2.241	[44a]
$[Mn_2(salmen)_2(N_3)_2]$	2.00	0.58	–	3.433	98.54	0	180	2.246	[44b]
$[Mn_2(acphpn)_2(N_3)_2]$	2.00	−0.20	–	3.425	101.23	0	180	2.202	[44c]
$[Mn_2(L)_2(N_3)_2]$	2.03	0.59	–	3.368	98.06	0	180	2.215	[45]
$[Mn_2(salpn)_2(N_3)_2]$	2.00	0.90	–	3.388	98.42	0	180	2.221	[46a]
$[Mn_2(salpn)_2(NCS)_2]$	2.01	0.14	–	3.369	99.39	0	180	2.192	[46b]
$[Mn_2(sapln)_2(H_2O)_2]$	2.00	1.10	–	3.315	99.50	0	180	2.158	[46c]
$[Mn_2(5\text{-Cl-sapln})_2(N_3)_2]$	1.95	1.79	–	3.440	101.42	0	180	2.210	[47]
$[Mn_2(acphen)_2(NCS)_2]$	2.00	−0.79	–	3.374	102.14	0	180	2.159	[48]

[a] Average values.

Table 4. Selected magneto- and structural parameters for type III Mn^{III} dinuclear complexes discussed in this work and elsewhere. Magnetic data is reported in the $\hat{H} = -2J\hat{S}_1 \cdot \hat{S}_{1\&}$ formalism.

Formula	g	*J* value (exptl) [cm^{-1}]	*J* value (calcd) [cm^{-1}]	Mn···Mn [Å]	Mn-O-Mn angle [Å][a]	Mn-O-Mn-O torsion	JT dihedral [Å]	Mn−O [Å][a]	Ref.
$[Mn_2(OMe)_2(L)(MeOH)](ClO_4)$	2.00	+6.25	+9.45	3.122	101.10	7.32	81.9	2.022	[49]
$[Mn_2(OMe)_2(HL)_4]$	1.90	+9.85	+9.8	3.084	102.51	2.20	117.1	1.976	[50]

[a] Average values.

and values of *J* even in borderline cases where the *J* values are less than 1 cm^{-1}.

To probe the electronic origin of the differences between the three types, a spin density plot has been computed for one structure from each type (**1**, II-**2** and III-**2**), as shown in Figure 6. The computed spin density of the metal atoms and the atoms which are coordinated to Mn^{III} for complexes **1**, II-**2** and III-**2** are listed in Table 5. The modulus of the spin densities on each manganese atom is calculated to be >3.7 in all three types, indicating that the magnetic orbitals are centred on the metals and that there is some unpaired spin density on the ligands. Generally, when the unpaired electrons are located in a metal π-type orbital (t_{2g}) spin polarization is expected to dominate, while if it is in a σ-type orbital a spin delocalization mechanism is expected to predominate. However this also then depends on the nature of the donor atoms.[15d] For Mn^{III} ions, since the unpaired electrons are located in three t_{2g}-like orbitals and in the d_z^2 orbital of the e_g set, a mechanism encompassing a mixture of spin delocalization and spin polarization is expected. As the Jahn–Teller axis coincides with the d_z^2 orbital direction, the ligand atoms which are coordinated via the Jahn–Teller axis are expected to have the positive spin density as here the spin delocalization will be predominant. In other directions, a mechanism comprising a mixture of spin delocalization and spin polarization is found, leading to either positive or negative spin densities on the donor atoms. In all three cases (**1**, II-**2** and III-**2**) the super-exchange propagates through the two bridging μ-alkoxo groups and the spin density on these bridging oxygen atoms is expected to influence the sign and magnitude of the *J* values.

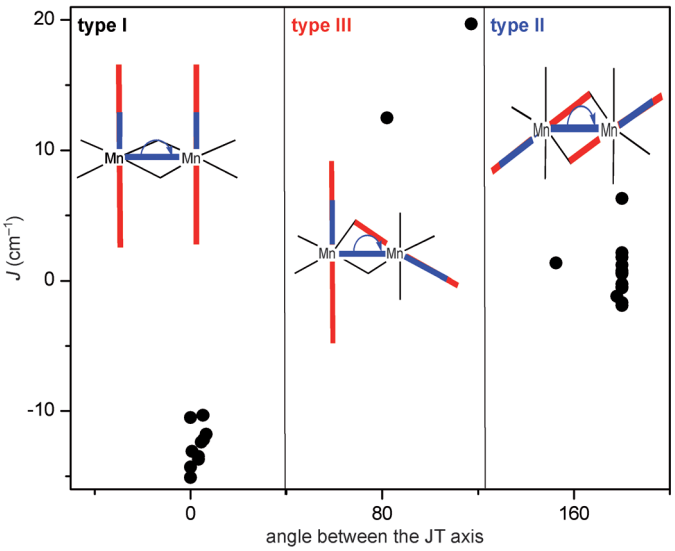

Figure 5. Plot of J (cm^{-1}) versus the angle forged between the two JT axes in Mn dimers of types I–III.

For type I structures, both μ-oxygen atoms have a very small positive spin density indicating that both the spin polarization and delocalization mechanisms compete, leading to very small spin densities on both oxygen atoms. In type II structures, since the Jahn–Teller axis is along the μ-O-atoms, a predominant spin delocalization from one of the Mn atoms and a mixture from the second Mn atom is expected, leading to a significant increase in the spin density compared to type I structures. In type III structures, since the Jahn–Teller axes are perpendicular, behaviour lying in-between that of type I and type II is observed, where one of the oxygen atoms (O23) has significant spin density, while the other (O24) has negligible spin density. These differences in the mechanism and differing magnitude of spin densities on the μ-alkoxo group is expected to be exemplified in the computed exchange interaction (Figure 6).[15d]

Orbital analysis: To probe the electronic origin further, molecular orbital (MO) analysis has been performed on complexes **1**, II-**2** and III-**2**. The DFT Kohn–Sham orbitals are very useful for qualitatively analysing the J values, and for providing some insight into the coupling mechanism. The qualitative model of Kahn-Briat[52] takes into consideration the overlap between the non-orthogonal magnetic orbitals

Table 5. DFT computed spin densities of selected atoms of complex **1**, II-**2** and III-**2**.

Complex (**1**)		Complex (II-**2**)		Complex (III-**2**)	
atom specification	spin densities	atom specification	spin densities	atom specification	spin densities
Mn1	3.9414	Mn1	3.7468	Mn1	3.8862
Mn2	3.9414	Mn2	3.7468	Mn2	3.8738
O3	0.0026	O3	0.0278	O11	−0.0028
O4	−0.0023	O6	0.0220	O14	−0.0045
O5	0.0114	O7	0.2793	O17	−0.0141
O6	0.0082	N8	−0.0833	O20	−0.0297
O7	0.0166	N9	−0.0561	O23	0.0379
O42	0.0026	O44	0.0278	O24	0.0069
O43	−0.0023	O45	0.0220	N26	0.0258
O44	0.0114	O46	0.2793	N28	0.0205
O45	0.0082	N47	−0.0803	N30	0.0040
O46	0.0166	N48	−0.0561	N32	−0.0283

and relates it to the J values. Even though types I–III differ in their net J values, the net exchange interactions have contributions from both the antiferromagnetic (J_{AF}) and ferromagnetic (J_F) parts. The computed overlap integral between the singly occupied orbitals is directly proportional to J_{AF}. It has been noted in several instances that the so-called cross-interaction between the empty $d_{x^2-y^2}$ orbitals and the singly occupied orbitals leads to ferromagnetic interactions and this has been qualitatively studied to rationalise the weak interactions observed in Mn^{III} dimers in general.[53] We have decided to compute the overlap integral for this pair, since its magnitude is expected to reveal the strength of the "cross-interaction" that exists in these molecules and thus can be translated as the contribution to J_F. The d-based orbitals of the alpha set for types I–III are shown in Figure 7. The results of the overlap integral calculation are summarised in the computed energy level diagram of Figure 8. A double-headed arrow connecting the alpha and beta sets indicates a significant overlap between the two orbitals (the grey arrows indicate significant cross-interaction). As is evident from the graph, type I structures have significant overlap with SOMOs but do not have any significant interaction with the $d_{x^2-y^2}$ orbitals leading to a decrease in the J_F contribution (See Tables S3–S7 in the Supporting Information for the complete list of computed overlap integrals). Among others, the d_{yz}-d_{yz}, d_{z^2}-d_{yz}, d_{yz}-d_{z^2}, d_{yz}-d_{xy}, d_{z^2}-d_{yz}, d_{xy}-d_{z^2} interactions are notable. A larger J_{AF} contribution and a negligible J_F contribution lead to a large antiferromagnetic net J

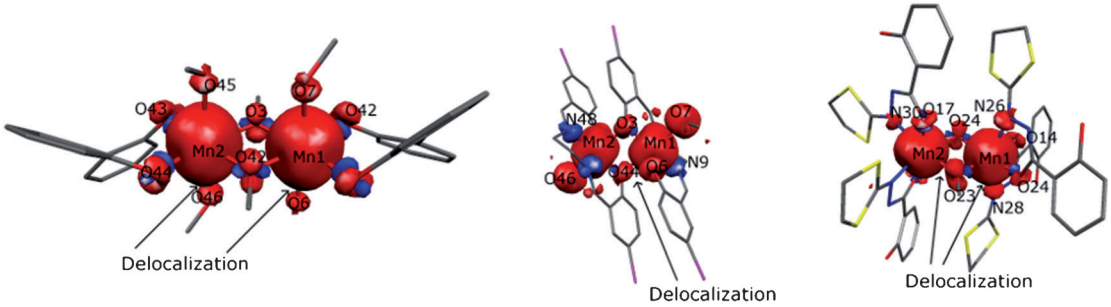

Figure 6. B3LYP computed spin density plot for **1**, II-**2** and III-**2** with a cut-off value of 0.005 a.u.

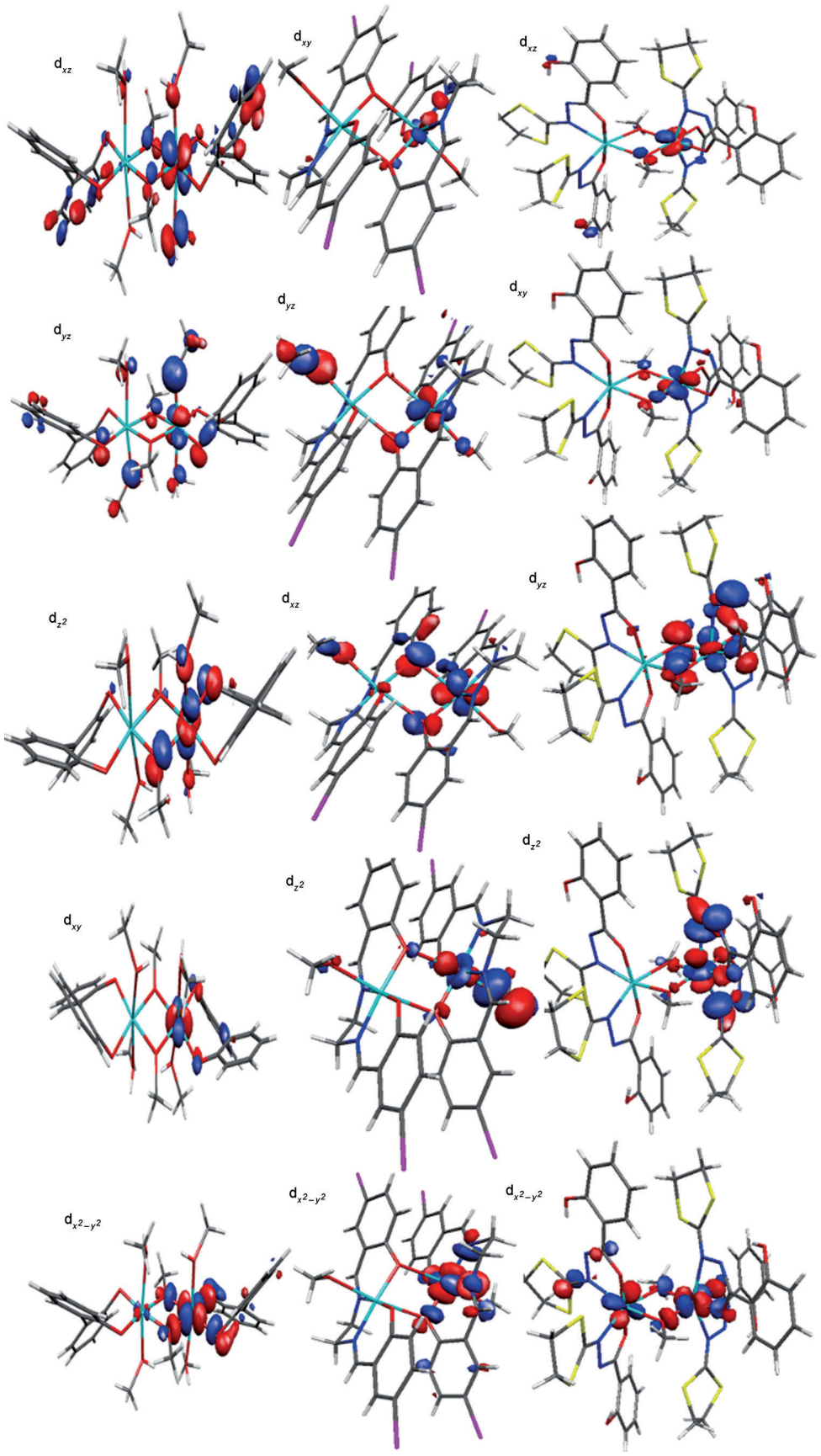

Figure 7. Alpha magnetic orbitals of types I, II and III in order of decreasing energy (top to bottom).

for this type of complex. For type II structures, both the J_F and J_{AF} contributions exist, with the significant exchanges being d_{yz}-d_{yz}, d_{xz}-d_{yz}, d_{yz}-d_{xz}, d_{xz}-d_{xz} and d_{xy}-d_{xy} along with some significant cross-interactions. Here the J_{AF} and J_F contributions essentially cancel each other out, leading to a very weak net exchange. The sign of the exchange (ferro or antiferro) in this type of complex is determined by the predominant factor. For type III structures on the other hand, fewer J_{AF} interactions are observed and the cross-interactions play a vital role. A large cross-interaction is evident from the broken symmetry $d_{x^2-y^2}$ orbital plotted in Figure 7. A stronger J_F and weaker J_{AF} leads to relatively strong net ferromagnetic exchange.

As mentioned before, the differences in the magnitude and the sign of J arise due to the difference in the orientation of the d_{z^2} orbital - which coincides with the Jahn–Teller axis. On several occasions the Jahn–Teller orientation has been evoked to explain the reduction in the cluster anisotropy and here for the first time with quantitative calculations and qualitative analysis, we provide direct evidence that the JT orientation is important in determining the sign as well as magnitude of the coupling in Mn^{III} dimers. A perpendicular alignment of the JT axes for the dinuclear unit is expected to exhibit a relatively strong ferromagnetic interaction. However we point out that this orientation is also likely to lead to a decrease in the cluster anisotropy, an important parameter to consider when designing molecular nanomagnets.

Since all of the complexes in this study possess different terminal ligands we then sought to determine the effect of

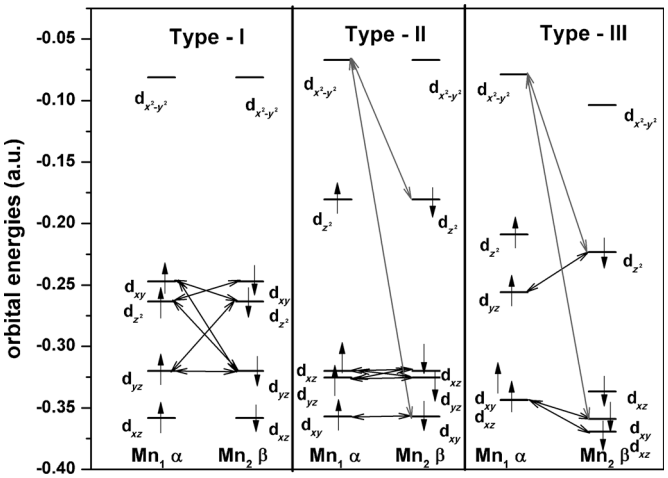

Figure 8. Dominant interactions between the magnetic orbitals in type I–III structures. Anti-ferromagnetic interactions are shown as black lines and ferromagnetic interactions as grey arrows.

a change in the nature of the terminal ligands on the J values. Thus we have modelled two complexes, in which the terminal ligands of complexes **1** and III-**2** were interchanged. This gives $J = -8.4\ cm^{-1}$ and $+21.6\ cm^{-1}$ compared to $-10.2\ cm^{-1}$ and $+9.8\ cm^{-1}$ for their original complexes, respectively. This clearly indicates that the terminal ligands have negligible contribution to the exchange coupling constant.

Magneto-structural correlations: Although the experimental studies and the theoretical analysis presented in this work strongly suggest that the orientation of the Jahn–Teller axis is the most important parameter in controlling J across the three types presented, within a particular type other structural parameters are expected to influence the final observed J value. Indeed, to our knowledge, no theoretical correlations have been developed for this topology to understand the unique structural features that are expected to affect the resultant J values. Here we have thus decided to develop correlations for a type I structure in the shape of our own complex **1** (Figure 1). There are four structural parameters deemed vital in influencing and determining the J value: Mn-O-Mn angle, Mn-O distance, Mn-O-Mn-O dihedral angle and the out-of-plane shift of the alkyl group (μ-OR) of the compound in question (described by τ). The developed correlations for these four parameters are given in Figure 9. The experimental parameters listed in Table 2 along with the experimental J have also been plotted along

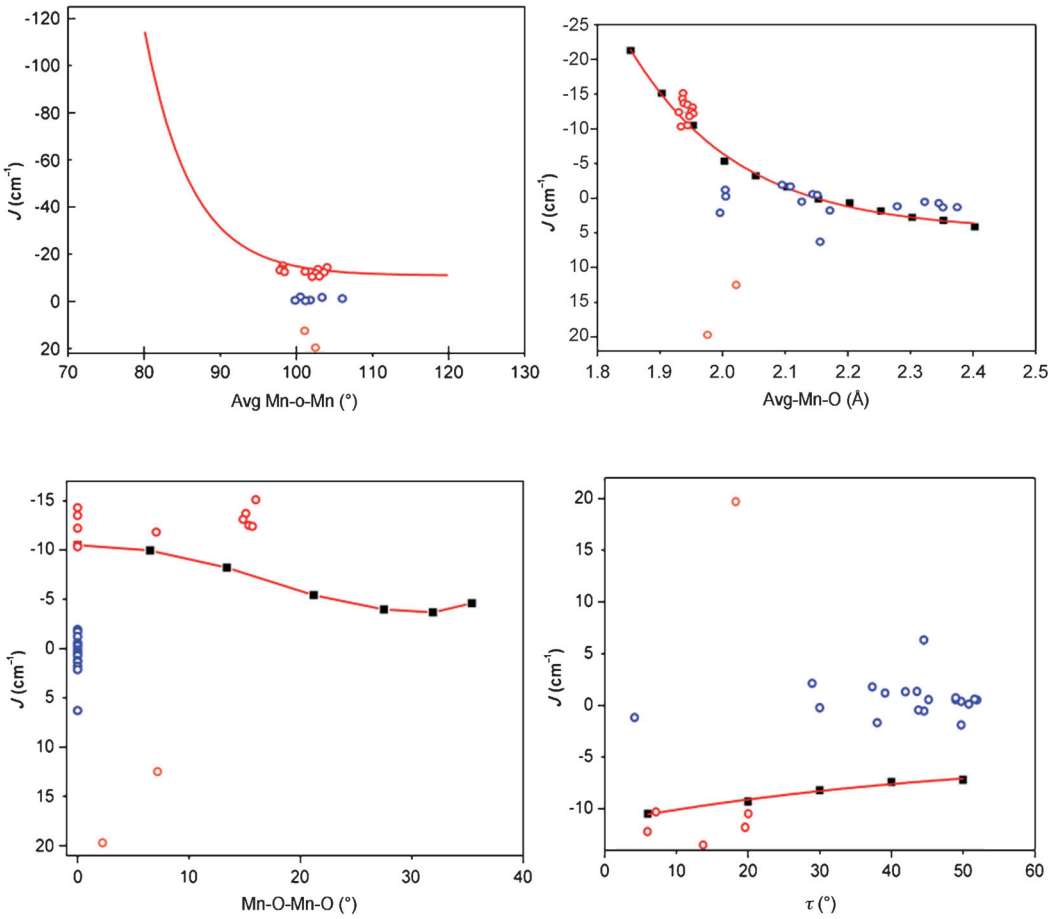

Figure 9. Magneto-structural correlations developed by varying structural parameters Mn-O-Mn and Mn-O-Mn-O angles, Mn-O distance and τ using DFT calculations. Experimental values are represented in coloured circles, red = type I, blue = type II, and orange = type III.

with the computed points (solid squares). For the data obtained from the experimental structure, the three types I–III are distinguished in different colours.

Bond angle: By varying the average Mn-O-Mn angle from 80.1° to 119.8°, a correlation has been developed for *J* and its value varies exponentially, as represented in Figure 9. The *J* parameter decreases and become less antiferromagnetic upon increasing Mn-O-Mn angle. At an acute angle, relatively strong antiferromagnetic exchange has been encountered with the steep increase in negative *J* due to significant overlap of the d_{xy} orbital with other orbitals, as evidenced from the overlap integral values (Table S3 in the Supporting Information). Since the Mn-O-Mn angle decreases with a decrease in the Mn···Mn distance, this effect is somewhat expected. However at large angles, an overall drop in the overlap values is detected and this leads to smaller negative *J* values. There is no switch from antiferromagnetic to ferromagnetic and this is essentially due to negligibly small cross-interactions at all the computed angles. The experimental type I data points lie within the computed points, revealing that this is a rather reliable parameter. As expected, type II and type III structures deviate from the computed data and this once again suggests that the JT orientation is more important than any other structural parameter.

Bond distance: The second correlation is carried out by varying the average Mn–O distances from 1.853 to 2.403 Å. This parameter also exhibits an exponential relationship (Figure 9) whereby the *J* value steadily decreases (becomes less antiferromagnetic) with increasing average distance. Moreover as the Mn–O distance passes a value of 2.103 Å, the interaction becomes ferromagnetic. This is because as the Mn–O distance increases, the type I structure will be converted into other types (II and III for example) and this leads to significant increase in cross interaction and a predominant ferromagnetic exchange. The experimental data points fit with the type I structures at shorter Mn–O distances and type II structures at longer Mn–O distances.

Dihedral angle: The Mn-O-Mn-O dihedral angle in **1** is varied from 0 to 35.4° to obtain the third correlation. The plot of dihedral angle versus *J* is shown in Figure 9. Only a small variation in *J* is detected and the complex becomes less ferromagnetic as the dihedral angle increases. This is as a result of the reduction in the d_{z^2}-d_{z^2} overlap. Here the experimental data points are rather scattered, suggesting that this parameter may not be particularly significant.

Out-of-plane displacement of methyl groups (τ): The fourth correlation analysis involved monitoring *J* when the out-of-plane displacement parameter (τ) of the bridging methyl O atoms was manipulated in the 6° to 50° range. The τ versus *J* plot (Figure 9) shows a linear relationship. As in the case of the dihedral correlation, an increase in the out-of plane displacement of the methyl group also leads to less antiferromagnetic *J* values, due to a reduction in overlap between the singly occupied orbitals of the Mn^{III} ions (Table S7 in the Supporting Information).

Conclusion

Based on the structural variation observed among the reported Mn^{III} dimeric structures having two alkoxide-bridges, a unique structural feature which distinguishes the type of magnetic interaction observed is proposed. This parameter, based on the orientation of the Jahn–Teller axes of the two Mn^{III} atoms, sharply categorises three different types of dimers where type I represent moderately strong antiferromagnetic exchange, type III structures exhibit moderately strong ferromagnetic interactions and type II structures are classified as borderline where a weak ferro- or antiferromagnetic interaction is detected. These three types of classification are supplemented with the synthesis and characterisation of a new family of alkoxide-bridged Mn^{III} dimers of general formula $[Mn^{III}_2(\mu\text{-}OR)_2(biphen)_2(ROH)_x(L)_y]$ (where R = Me, Et; H_2biphen = 2,2′-biphenol and L = terminally bonded N-donor ligand). All five structures reported here belong to type I and help us to extend the database to validate the proposed correlations. Additionally, a detailed computational study on all three types was undertaken to probe the electronic origin of the differences in the magnetic behaviour observed. Our computations reveal that the magnetic exchange interaction has two contributions, J_{AF} and J_F, with the J_F contribution arising due to the cross interaction between the SOMOs and the unoccupied d orbitals. The strength of J_F is vital as it determines the sign and magnitude of the *J* observed in all three types. However the strength of J_F is related to the orientation of the d_{z^2} orbitals in a particular structure. Since the orientation of the d_{z^2} orbital is related to the Jahn–Teller elongation, our study reveals that a perpendicular orientation of the d_{z^2} orbitals enhances J_F significantly, leading to a strong ferromagnetic interaction (type III). A parallel orientation of the two Jahn–Teller axes which lie in the bridging plane is found to be a borderline case (type II). If these axes do not form the μ-alkoxide bridges, then a moderately strong antiferromagnetic interaction is encountered (type I). The electronic origins of these differences were traced back to the orbital overlaps and this has been quantitatively analysed using overlap integral computation.

In the field of molecular magnetism a strong ferromagnetic interaction is a highly sought-after parameter as the ferromagnetic interaction maximises the ground state *S* value and its strength helps to promote an isolated ground state. Although a plethora of SMMs comprising Mn^{III} ions have been reported, there have been no extensive studies undertaken to pinpoint the unique structural features which would yield this highly sought-after parameter. The combined experimental and theoretical study undertaken here reveals that the orientation of Jahn–Teller axes plays an important role in the magnetic coupling, with a perpendicular orientation

leading to a strong ferromagnetic exchange. However, it is well known that a perpendicular orientation of Jahn–Teller axes leads to a decrease in the anisotropy of the cluster, which is an important parameter in designing molecular nanomagnets. Our study therefore suggests that large anisotropy and a strong ferromagnetic interaction are unlikely to coexist in Mn^{III} clusters containing only $[Mn(\mu\text{-}OR)]_2$ building blocks.

Experimental Section

Physical measurements: Infrared spectra were recorded on a Perkin–Elmer FT-IR Spectrum One spectrometer equipped with a Universal ATR Sampling accessory (NUI Galway). Elemental analysis detailed was carried out by Marion Vignoles of the School of Chemistry microanalysis service at NUI Galway. Variable-temperature, solid-state direct current (dc) magnetic susceptibility data down to 1.8 K were collected on a Quantum Design MPMS-XL SQUID magnetometer equipped with a 7 T dc magnet (University of Edinburgh). Diamagnetic corrections were applied to the observed paramagnetic susceptibilities using Pascal's constants.

X-Ray crystallography: The structures of **1–5** were collected on an Xcalibur S single crystal diffractometer (Oxford Diffraction) using an enhanced Mo source. Each data reduction was carried out on the CrysAlisPro software package. For more detailed refinement information please consult the ESI. Full details can also be found in the CIF files: CCDC-843730 (**1**), CCDC-843731 (**2**), CCDC-843732 (**3**), CCDC-843733 (**4**), CCDC-843849 (**5**), contain the supplementary crystallographic data for this paper. These data can be obtained free of charge from The Cambridge Crystallographic Data Centre via www.ccdc.cam.ac.uk/data_request/cif.

Computational details: All calculations were performed using the hybrid B3LYP[54] functional with Alhrich[54] triple- ζ basis set as implemented in the Gaussian 09[55] suite of programs. The *J* values were computed from the energy differences between the high spin (EHS) state calculated using single determinant wave functions, and the low spin (EBS) state determined using the Broken Symmetry (BS) approach developed by Noodleman.[56] Negative and positive values for *J* correspond to antiferromagnetic and ferromagnetic interactions, respectively. Details of the computational method employed to compute the exchange interaction is discussed elsewhere.[57]

Syntheses: All reactions were performed under aerobic conditions at room temperature and all reagents and solvents were used as purchased. Caution: Due care and attention should be given when working with the potentially explosive perchlorate and nitrate salts.

Preparation of $[Mn^{III}_2(\mu\text{-}OMe)_2(biphen)_2(MeOH)_4]$ (1): A 1.456 M aqueous solution of $Mn(NO_3)_2{\cdot}6H_2O$ (2 cm^3, 2.9 mmol) and 2,2′-biphenol (0.54 g, 2.9 mmol) were dissolved in MeOH (30 cm^3). NaOH (0.115 g, 2.9 mmol) was then added and the solution was left stirring for 10 min. The resultant deep brown solution was then filtered and allowed to stand. X-ray quality crystals of **1** were obtained upon slow evaporation of the mother liquor overnight. FT-IR (KBr): $\tilde{\nu}$ = 3056.0(w), 1587.6(w), 1488.8(m), 1469.2(m), 1430.8(s), 1250.6(s), 1220.9(s), 1154.1(w), 1118.1(w), 1096.2(w), 1046.8(w), 1007.6(w), 934.0(w), 857.8(s), 836.6(m), 753.1(vs), 728.0(s), 710.0 cm^{-1}(m); elemental analysis calcd (%) for $C_{30}H_{38}O_{10}Mn_2$: C 53.90, H 5.73; found: C 53.82, H 5.93.

Preparation of $[Mn^{III}_2(\mu\text{-}OMe)_2(biphen)_2(py)_3]$ (2): $MnBr_2{\cdot}4H_2O$ (0.5 g, 1.74 mmol) and 2,2′-biphenol (0.32 g, 1.74 mmol) were dissolved in MeOH (40 cm^3). $NaOPh{\cdot}3H_2O$ (0.15 g, 0.87 mmol) and NaOH (0.035 g, 0.87 mmol) were then added and the resultant deep brown solution was stirred for 15 min. After this time an excess of pyridine was added (12 cm^3, 149 mmol) and the mixture was left stirring for a further 10 min. The solution was then filtered and left to stand in a fume-cupboard covered by a perforated lid. X-ray quality crystals of **2** were obtained upon slow evaporation of the mother liquor after two days. FT-IR (KBr): $\tilde{\nu}$ = 3060.7(w), 3003.3(w), 2920.9(w), 2815.5(w), 1595.7(m), 1585.2(w), 15578.0(w), 1486.7(m), 1464.3(m), 1443.2(m), 1431.3(s), 1357.5(w), 1292.4(w), 1256.9(s), 1212.0(s), 1152.2(w), 1113.3(w), 1096.5(w), 1053.4(s), 1035.6(m), 1003.4(m), 932.8(w), 857.4(s), 832.7(m), 768.1(s), 755.0(m), 731.8(m), 698.6 cm^{-1}(s); elemental analysis calcd (%) for $C_{41}H_{37}O_6N_3Mn_2$: C 63.33, H 4.80, N 5.40; found: C 63.28, H 4.76, N 5.48.

Preparation of $[Mn^{III}_2(\mu\text{-}OMe)_2(biphen)_2(3\text{-}pic)_2].2H_2O$ (3): $MnBr_2{\cdot}4H_2O$ (0.167 g, 0.58 mmol) and 2,2′-biphenol (0.11 g, 0.59 mmol) were dissolved in MeOH (20 cm^3). $NaOPh.3H_2O$ (0.05 g, 0.43 mmol) and NaOH (0.012 g, 0.3 mmol) were then added in sequence, and the solution was left stirring for 5 min. After this time an excess of 3-picoline (2 cm^3, 20.55 mmol) was added and the reactant mixture was allowed to stir for a further 15 min. The resultant deep brown solution was then filtered, covered with a perforated lid and allowed to stand in the fume-cupboard. X-ray quality crystals of **3** were obtained upon slow evaporation of the mother liquor after 24 h. FT-IR (KBr): $\tilde{\nu}$ = 3050.9(w), 2922.7(w), 2819.7(w), 1738.3(w), 1581.9(w), 1485.0(m), 1461.6(m), 1428.0(s), 1272.1(m), 1255.8(s), 1221.8(s), 1193.0(m), 1096.6(w), 1053.0(m), 1003.7(m), 935.9(w), 866.8(m), 832.7(m), 798.2(m), 761.4(vs), 726.3(s), 703.5 cm^{-1}(s); elemental analysis calcd (%) for $C_{38}H_{36}O_6N_2Mn_2$: C 62.82, H 4.99, N 3.83; found: C 62.77, H 5.02, N 8.63.

Preparation of $[Mn^{III}_2(\mu\text{-}OEt)_2(biphen)_2(3\text{-}pic)_2]$ (4): $MnBr_2{\cdot}4H_2O$ (0.5 g, 1.74 mmol) and 2,2′-biphenol (0.32 g, 1.72 mmol) were dissolved in EtOH (40 cm^3). Sequentially, NaOMe (0.28 g, 5.2 mmol) and 3-picoline (2 cm^3, 20.55 mmol) were added and the solution was left stirring for 10 min. The resultant deep brown solution was then filtered, covered with a perforated lid and allowed to stand in the fume-cupboard. X-ray quality crystals of **4** were obtained upon slow evaporation of the mother liquor after 24 h. FT-IR (KBr): $\tilde{\nu}$ = 3052.2(w), 2969.6(w), 2927.7(w), 1625.2(w), 1581.9(m), 1486.6(m), 1464.6(m), 1427.4(s), 1382.7(m), 1273.5(m), 1258.4(s), 1225.5(s), 1194.0(m), 1152.5(w), 1127.4(w), 1087.8(m), 1037.5(s), 1003.5(m), 935.4(w), 889.1(m), 869.2(s), 858.9(m), 835.3(m), 797.1(m), 763.7(vs), 728.7(m), 712.9(m), 703.6(s), 653.1 cm^{-1}(m); elemental analysis calcd (%) for $C_{40}H_{40}O_6N_2Mn_2$: C 63.66, H 5.34, N 3.71; found: C 63.82, H 5.28, N 4.04.

Preparation of $[Mn^{III}_2(\mu\text{-}OEt)_2(biphen)_2(1\text{-}OH\text{-}py)_2(EtOH)_2]$ (5): $Mn(ClO_4)_2{\cdot}6H_2O$ (0.35 g, 0.96 mmol) and 2,2′-biphenol (0.26 g, 1.4 mmol) were dissolved in EtOH (40 cm^3). The ligand 2-hydroxypyridine (0.26 g, 2.74 mmol) and $NMe_4(OH)$ (0.25 g, 2.75 mmol) were then added in sequence and the resultant deep brown solution was left to stir for 10 min. After this time the solution was filtered, covered with a perforated lid and allowed to stand in the fume hood for several days. X-ray quality crystals of **5** were obtained upon slow evaporation of the mother liquor after two days. FT-IR (KBr): $\tilde{\nu}$ = 3254.6(w), 3047.6(w), 2920.5(w), 1695.8(w), 1642.8(vs), 1606.9(s), 1537.4(m), 1487.1(m), 1470.0(m), 1430.7(s), 1406.1(m), 1376.1(m), 1274.6(s), 1261.4(m), 1233.2(s), 1154.3(m), 1093.0(m), 1044.4(s), 992.2(m), 963.4(w), 933.1(w), 895.0(m), 866.6(m), 841.3(m), 762.6(vs), 727.8(s), 711.6(m), 669.0 cm^{-1}(w); elemental analysis calcd (%) for $C_{42}H_{48}O_{10}N_2Mn_2$: C 59.30, H 5.69, N 3.29; found: C 59.35, H 5.67, N 3.16.

Acknowledgements

We would like to thank the IRSCET Embark Program (NB) and the NUI Galway Millennium Fund (LFJ) for funding. G.R. and T.R. (J.R.F.) would like to acknowledge financial support from the Government of India through Department of Science and Technology (SR/S1/IC-41/2010) and Indian Institute of Technology Bombay for computing time. E.K.B. acknowledges the financial support of the EPSRC and the Leverhulme Trust.

[1] O. Kahn, *Angew. Chem.* **1985**, *97*, 837; *Angew. Chem. Int. Ed.* **1985**, *24*, 834.

[2] a) L. Bogani, W. Wernsdorfer, *Nat. Mater.* **2008**, *7*, 179–186; b) M. N. Leuenberger, D. Loss, *Nature* **2001**, *410*, 789–793;

c) R. E. P. Winpenny, *Angew. Chem.* **2008**, *120*, 8112–8114; *Angew. Chem. Int. Ed.* **2008**, *47*, 7992–7994; d) M. Evangelisti, E. K. Brechin, *Dalton Trans.* **2010**, *39*, 4672–4676.
[3] B. C. Guha, *Proc. R. SOC. London Ser. A* **1951**, *206*, 353–373.
[4] B. Bleaney, K. D. Bowers, *Proc. R. SOC. London Ser. A* **1952**, *214*, 451–465.
[5] J. N. Van Niekerk, F. K. L. Schoening, *Acta Crystallogr.* **1953**, *6*, 227–232.
[6] a) W. E. Hatfield, *ACS Symp. Ser.* 5, **1974**, 108; b) D. J. Hodgson, *Prog. Inorg. Chem.* **1975**, *19*, 173; c) K. T. McGregor, N. T. Watkins D. L. Lewis, R. F. Drake, D. J. Hodgson, W. E. Hatfield, *Inorg. Nucl. Chem. Lett.* **1973**, *9*, 423; d) D. L. Lewis, K. T. McGregor, W. E. Hatfield, D. J. Hodgson, *Inorg. Chem.* **1974**, *13*, 1013; e) E. D. Estes, W. E. Hatfield, D. J. Hodgson, *Inorg. Chem.* **1974**, *13*, 1654.
[7] a) W. E. Marsh, K. C. Patel, W. E. Hatfield, D. J. Hodgson, *Inorg. Chem.* **1983**, *22*, 511–515; b) C. P. Landee, R. E. Greeney, *Inorg. Chem.* **1986**, *25*, 3771–3775.
[8] R. Costa, I. de. P. H. Moriera, S. Youngme, K. Siriwong, N. Wannarit, F. Ilias, *Inorg. Chem.* **2010**, *49*, 285–294.
[9] S. S. Tandon, L. K. Thompson, M. E. Manuel, J. N. Bridson, *Inorg. Chem.* **1994**, *33*, 5555–5570.
[10] a) S. M. Gorun, S. J. Lippard, *Inorg. Chem.* **1991**, *30*, 1625–1630; b) R. Werner, S. Ostrovsky, K. Griesar, W. Haase, *Inorg. Chim. Acta* **2001**, *326*, 78–88; c) H. Weihe, H. U. Güdel, *J. Am. Chem. Soc.* **1997**, *119*, 6539–6543; d) H. Weihe, H. U. Güdel, *J. Am. Chem. Soc.* **1998**, *120*, 2870–2879.
[11] a) W. E. Hatfield, J. J. MacDougall, R. E. Sheperd, *Inorg. Chem.* **1981**, *20*, 4216–4219; b) R. P. Scaringe, D. J. Hodgson, W. E. Hatfield, *Transition Met. Chem.* **1981**, *6*, 340–344; c) S. Cline, D. J. Hodgson, S. Kallesøe, S. Larsen, E. Pedersen, *Inorg. Chem.* **1983**, *22*, 637–642; d) D. J. Hodgson, *NATO ASI Ser., Ser. C* **1985**, *140*, 497–522.
[12] a) T. K. Karmakar, B. K. Ghosh, A. Usman, H.-K. Fun, E. Riviere, T. Mallah, G. Aromi, S. K. Chandra, *Inorg. Chem.* **2005**, *44*, 2391–2399.
[13] D. A. Pantazis, V. Krewald, M. Orio, F. Neese, *Dalton Trans.* **2010**, *39*, 4959–4967.
[14] a) R. Sessoli, D. Gatteschi, A. Caneshi, M. A. Novak, *Nature* **1993**, *365*, 141; b) R. Sessoli, H.-L. Tsai, A. R. Schake, S. Wang, J. B. Vincent, K. Folting, D. Gatteschi, G. Christou, D. N. Hendrickson, *J. Am. Chem. Soc.* **1993**, *115*, 1804.
[15] a) T. Cauchy, E. Ruiz, S. Alvarez, *J. Am. Chem. Soc.* **2006**, *128*, 15722; b) E. Ruiz, *Struct. Bonding (Berlin)* **2004**, *113*, 71; c) P. J. Hay, J. C. Thibeault, R. Hoffmann, *J. Am. Chem. Soc.* **1975**, *97*, 4884; d) O. Kahn, B. Briat, *J. Chem. Soc. Faraday Trans. 2* **1976**, *72*, 268.
[16] a) S. Gehring, P. Fleischhauer, H. Paulus, W. Haase, *Inorg. Chem.* **1993**, *32*, 54–60; b) Y.-Q. Zhang, C.-L. Luo, *Dalton Trans.* **2009**, 5627–5636.
[17] a) J. Tercero, E. Ruiz, S. Alvarez, A. Rodriguez-Fortea, P. Alemany, *J. Mater. Chem.* **2006**, *16*, 2729–2735; b) L. Gregoli, C. Danieli, A. Laure-Barre, P. Neugebauer, G. Pellegrino, G. Poneti, R. Sessoli, A. Cornia, *Chem. Eur. J.* **2009**, *15*, 6456–6467; c) M. A. Palacios, A. J. Mota, J. E. Perea-Buceta, F. E. White, E. K. Brechin, E. Colacio, *Inorg. Chem.* **2010**, *49*, 10156–10165; d) S. Sasmal, S. Hazra, P. Kundu, S. Majumder, N. Aliaga-Alcalde, E. Ruiz, S. Mohanta, *Inorg. Chem.* **2010**, *49*, 9517–9526.
[18] a) C. J. Milios, R. Inglis, A. Vinslava, R. Bagai, W. Wernsdorfer, S. Parsons, S. P. Perlepes, E. K. Brechin, *J. Am. Chem. Soc.* **2007**, *129*, 12505–12511; b) A. Prescimone, C. J. Milios, J. Sanchez-Benitez, K. V. Kamenev, C. Loose, J. Kortus, S. Moggach, M. Murrie, J. E. Warren, E. K. Brechin, *Dalton Trans.* **2009**, 4858–4867; c) R. Inglis, L. F. Jones, C. J. Milios, S. Datta, A. Collins, S. Parsons, W. Wernsdorfer, S. Hill, S. P. Perlepes, S. Piligkos, E. K. Brechin, *Dalton Trans.* **2009**, 3403–3412.
[19] O. Waldmann, R. Koch, S. Schromm, J. Schulein, P. Muller, I. Bernt, R. W. Saalfrank, F. Hampel, E. Balthes, *Inorg. Chem.* **2001**, *40*, 2986–2995.
[20] a) J. Bartolomé, G. Filoti, V. Kunscer, G. Schinteie, V. Mereacre, C. E. Anson, A. K. Powell, D. Prodius, C. Turta, *Phys. Rev. B* **2009**, *80*, 014430; b) G. Rajaraman, F. Totti, A. Bencini, A. Caneschi, R. Sessoli, D. Gatteschi, *Dalton Trans.* **2009**, 3153–3161.
[21] E. Ruiz, S. Alvarez, A. Rodriguez-Fortea, P. Alemany, Y. Pouillon, C. Massobrio, in *From Magnetism: Molecules to Materials II*, (Eds.: J. S. Miller, M. Drillon), Wiley-VCH, Weinheim, **2001**, pp. 227–279.
[22] G. Aromi, E. K. Brechin, *Struct. Bonding (Berlin)* **2006**, 122, 1–67.
[23] For examples of the first row coordination chemistry of the 2,2′-biphenolate ligand see: a) N. Berg, L. F. Jones, *CrystEngComm* **2010**, *12*, 3518–3521; b) N. Berg, L. F. Jones, *CrystEngComm* **2011**, *13*, 5510–5518; c) D. P. Goldberg, A. Caneschi, S. J. Lippard, *J. Am. Chem. Soc.* **1993**, *115*, 9299–9300; d) D. P. Goldberg, A. Caneschi, C. D. Delfs R. Sessoli, S. J. Lippard, *J. Am. Chem. Soc.* **1995**, *117*, 5789–5800; e) A. R. Schake, E. A. Schmitt, A. J. Conti, W. E. Strieb, J. C. Huffman, D. N. Hendrickson, G. Christou, *Inorg. Chem.* **1991**, *30*, 3192–3199; f) E. W. Ainscough, A. M. Brodie, S. J. McLachlan, K. L. Brown, *J. Chem. Soc. Dalton Trans.* **1983**, 1385–1389; g) J. S. Bashkin, A. N. Schake, J. B. Vincent, H.-R. Chang, Q. Li, J. C. Huffmann, G. Christou, D. N. Hendrickson, *J. Chem. Soc. Chem. Commun.* **1988**, 700–702.
[24] A. W. Addison, T. N. Rao, J. Reedjijk, J. van Rijn and G. C. Verschoor, *J. Chem. Soc. Dalton Trans.* **1984**, *7*, 1349–1356.
[25] H. Biava, C. Palopoli. S. Shova. M. De Gaudio. V. Daier, M. González-Sierra. J. P. Tuchagues. S. Signorella, *J. Inorg. Biochem.* **2006**, *100*, 1660–1671.
[26] C. Palopoli. M. González-Sierra, G. Robles, F. Dahan, J. P. Tuchagues, S. Signorella, *Dalton Trans.* **2002**, 3813–3819.
[27] V. Daier. H. Biava, C. Palopoli. S. Shova. J. P. Tuchagues. S. Signorella, *J. Inorg. Biochem.* **2004**, *98*, 1806–1817.
[28] T. K. Paine, T. Weyhermüller. E. Bothe, K. Wieghardt, P. Chaudhuri, *Dalton Trans.* **2003**, 3136–3144.
[29] D. Moreno, C. Palopoli, V. Daier, S. Shova, L. Vendier. M. González-Sierra, J. P. Tuchagues, S. Signorella, *Dalton Trans.* **2006**, 5156–5166.
[30] M. Mikuriya, Y. Yamoto, *Inorg. Chim. Acta* **1991**, *181*, 1–2.
[31] X. Shi Tan, W. X. Tang, *Polyhedron* **1996**, *15*, 2671–2675.
[32] J.-J. Zhang. Q.-H. Luo, C.-Y. Duan, Z.-L. Wang, Y.-H. Mei, *J. Inorg. Biochem.* **2001**, *86*, 573–579.
[33] H. Miyasaka, R. Clerac, W. Wernsdorfer, L. Lecren, C. Bonhomme. K.-I. Sugiura, M. Yamashita, *Angew. Chem.* **2004**, *116*, 2861–2865; *Angew. Chem. Int. Ed.* **2004**, *43*, 2801–2805.
[34] H.-L. Shyu, H.-H. Wei, Y. Wang, *Inorg. Chim. Acta* **1999**, *290*, 8–13.
[35] Z. Lü, M. Yuan, F. Pan, S. Gao. D. Zhang, D. Zhu, *Inorg. Chem.* **2006**, *45*, 3538–3548.
[36] N. Matsumoto, Z.-J. Zhong, H. Okawa, S. Kida, *Inorg. Chim. Acta* **1989**, *160*, 153–157.
[37] G. Rajaraman. E. Carolina Sanudo. M. Helliwell, S. Piligkos. W. Wernsdorfer. G. Christou, E. K. Brechin, *Polyhedron* **2005**, *24*, 2450–2454.
[38] S. Saha, D. Mal, S. Koner. A. Bhattacherjee, P. Gütlich, S. Mondal, M. Mukherjee, K.-I. Okamoto, *Polyhedron* **2004**, *23*, 1811–1817.
[39] G. L. Abbati, A. Cornia, A. C. Fabretti, A. Caneschi, D. Gatteschi, *Inorg. Chem.* **1998**, *37*, 3759–3766.
[40] A. Gelasco, M. L. Kirk, J. W. Kampf, V. L. Pecoraro, *Inorg. Chem.* **1997**, *36*, 1829–1837.
[41] J.-J. Zhang, Y.-Y. Tang, Q.-H. Luo, C.-Y. Duan, Z.-L. Wang, Y.-H. Mei, *Polyhedron* **2001**, *20*, 2285–2291.
[42] H. Miyasaka, R. Clerac, T. Ishii, H.-C. Chang, S. Kitagawa, M. Yamashita, *Chem. Soc. Dalton Trans.* **2002**, 1528–1534.
[43] Z.-Y. Zhang, C. Brouca-Cabarrecq, C. Hemmert, F. Dahan, J.-P. Tuchagues, *J. Chem. Soc. Dalton Trans.* **1995**, 1453–11460.
[44] G. Bhargavi, M. V. Rajeskharan, J.-P. Costes, J.-P. Tuchagues, *Polyhedron* **2009**, *28*, 1253–1260.
[45] S. Mandal, G. Rosair, J. Ribas, D. Bandyopadhay, *Inorg. Chim. Acta* **2009**, *362*, 2200–2204.
[46] Y. Feng, C. Wang, Y. Zhao, J. Li, D. Liao, S. Yan, Q. Wang, *Inorg. Chim. Acta* **2009**, *362*, 3563–3568.

[47] J. H. Belser, D. W. Ryu, H. C. Kim, S. W. Yoon, B. J. Suh, C. S. Hong, *Angew. Chem.* **2009**, *121*, 3715–3718; *Angew. Chem. Int. Ed.* **2009**, *48*, 3661–3664.
[48] G. Bhagravi, M. V. Rajasekharan, J.-P. Tuchagues, *Inorg. Chim. Acta* **2009**, *362*, 3247–3252.
[49] M. F. Anderlund, J. Zheng, M. Ghiladi, M. Kritikos, E. Rivière, L. Sun, J.-J. Girerd, B. Akermark, *Inorg. Chem. Commun.* **2006**, *9*, 1195–1198.
[50] C. Beghidja, G. Rogez, J. Kortus, M. Wesolek, R. Welter, *J. Am. Chem. Soc.* **2006**, *128*, 3140–3141.
[51] a) R. Celenligil-Cetin, P. Paraskevopoulou, N. Lalioti, Y. Sanakis, R. J. Staples, N. P. Rath, P. Stavropoulus, *Inorg. Chem.* **2008**, *47*, 10998–11009; b) L. Dubois, J. Pécaut, M.-F. Charlot, C. Baffert, C. Collomb, M. N. Deronzier, J. M. Latour, *Chem. Eur. J.* **2008**, *14*, 3013–3025; c) Y. Mikata, H. So, A. Yamashita, A. Kawamura, M. Mikuriya, K. Fukui, A. Ichimura, S. Yano, *Dalton Trans.* **2007**, 3300–3334; d) J. Glerup, P. A. Goodson, A. Hazell, R. Hazell, D. J. Hodgson, C. J. McKenzie, K. Nichelsen, U. Rychlewska, H. Toftlund, *Inorg. Chem.* **1994**, *33*, 4105–4111.
[52] A. D. Becke, *J. Chem. Phys.* **1993**, *98*, 5648–5652.
[53] R. Hotzelmann, K. Wieghardt, U. Florke, H.-J. Haupt, D. C. Weatherburn, J. Jacques Bonvoisin, G. Genevibe Blondin, J.-J. Girerd, *J. Am. Chem. Soc.* **1992**, *114*, 1681–1696.
[54] a) A. Schäfer, H. Horn, R. Ahlrichs, *J. Chem. Phys.* **1992**, *97*, 2571–2577; b) A. Schäfer, C. Huber, R. Ahlrichs, *J. Chem. Phys.* **1994**, *100*, 5829–5835.
[55] *Gaussian 09*, *Revision A.02*, M. J. Frisch, G. W. Trucks, H. B. Schlegel, G. E. Scuseria, M. A. Robb, J. R. Cheeseman, G. Scalmani, V. Barone, B. Mennucci, G. A. Petersson, H. Nakatsuji, M. Caricato, X. Li, H. P. Hratchian, A. F. Izmaylov, J. Bloino, G. Zheng, J. L. Sonnenberg, M. Hada, M. Ehara, K. Toyota, R. Fukuda, J. Hasegawa, M. Ishida, T. Nakajima, Y. Honda, O. Kitao, H. Nakai, T. Vreven, J. A. Montgomery, Jr., J. E. Peralta, F. Ogliaro, M. Bearpark, J. J. Heyd, E. Brothers, K. N. Kudin, V. N. Staroverov, R. Kobayashi, J. Normand, K. Raghavachari, A. Rendell, J. C. Burant, S. S. Iyengar, J. Tomasi, M. Cossi, N. Rega, J. M. Millam, M. Klene, J. E. Knox, J. B. Cross, V. Bakken, C. Adamo, J. Jaramillo, R. Gomperts, R. E. Stratmann, O. Yazyev, A. J. Austin, R. Cammi, C. Pomelli, J. W. Ochterski, R. L. Martin, K. Morokuma, V. G. Zakrzewski, G. A. Voth, P. Salvador, J. J. Dannenberg, S. Dapprich, A. D. Daniels, O. Farkas, J. B. Foresman, J. V. Ortiz, J. Cioslowski, and D. J. Fox, Gaussian, Inc., Wallingford CT, **2009**.
[56] L. Noodleman, *J. Chem. Phys.* **1981**, *74*, 5737–5743.
[57] a) E. Ruiz, S. Alvarez, J. Cano, P. Alemany, *J. Comput. Chem.* **1999**, *20*, 1391–1400; b) E. Ruiz, A. Rodriguez-Fortea, J. Cano, S. Alvarez, P. Alemany, *J. Comput. Chem.* **2003**, *24*, 982–989; c) G. Rajaraman, J. Cano, E. K. Brechin, E. J. L. McInnes, *Chem. Commun.* **2004**, 1476–1477; d) P. Christian, G. Rajaraman, A. Harrison, J. J. W. McDouall, J. Raftery, R. E. P. Winpenny, *Dalton Trans.* **2004**, 2550–2555; e) G. Rajaraman, M. Murugesu, E. C. Sanudo, M. Soler, W. Wernsdorfer, M. Helliwell, C. Muryn, J. Raftery, S. J. Teat, G. Christou, E. K. Brechin, *J. Am. Chem. Soc.* **2004**, *126*, 15445–15457; f) A. Bencini, F. Totti, *Int. J. Quantum Chem.* **2005**, *101*, 819–825; g) K. Hegetschweiler, B. Morenstern, J. Zubieta, P. J. Hagrman, N. Lima, R. Sessoli, F. Totti, *Angew. Chem.* **2004**, *116*, 3518–3521; *Angew. Chem. Int. Ed.* **2004**, *43*, 3436–3439.

Received: September 9, 2011
Revised: December 12, 2011
Published online: March 29, 2012

